Illuminating N-acylethanolamine biosynthesis with new chemical tools

Mock, E.D.

Chapter 5

LEI-401 is an *in vivo* active NAPE-PLD inhibitor that reduces brain anandamide levels and pain behavior

5.1 Introduction

In recent years lipids have come to the foreground as signaling mediators in the central nervous system (CNS).[1-4] While classical neurotransmitters are stored in synaptic vesicles and released upon fusion with the plasma membrane of neurons, due to their lipophilic nature, lipids readily diffuse through membranes and are not stored in vesicles. It is, therefore, generally accepted that signaling lipids are produced 'on demand' and are rapidly metabolized to terminate their biological action.[5] In particular, the endocannabinoid anandamide (*N*-arachidonoylethanolamine, AEA) has emerged as a key lipid that regulates neurotransmission via its interaction with the cannabinoid CB_1 receptor and ion channels, such as the *N*-methyl-D-aspartate (NMDA) receptor[6], T-type Ca^{2+} channels[7], the acid-sensitive background K^+ channel (TASK-1)[8] and transient receptor potential vanilloid type 1 (TRPV1)[9]. Genetic deletion or pharmacological inhibition of the anandamide degrading enzyme, fatty acid amide hydrolase (FAAH), has revealed that elevated anandamide levels modulate various physiological processes such as pain[10],

anxiety[11], appetite[12] and inflammation[13]. The physiological effects resulting from perturbation of anandamide biosynthesis in living systems are, however, poorly studied, partly because of a lack of pharmacological tools that can modulate the enzymes involved in anandamide production.[14]

N-acylphosphatidylethanolamine phospholipase D (NAPE-PLD) is generally considered the major anandamide biosynthetic enzyme.[15,16] Biochemical and structural studies have demonstrated that NAPE-PLD is a membrane-associated, constitutively active zinc hydrolase with a metallo-β-lactamase fold.[17] The enzyme generates a family of bioactive lipids, termed *N*-acylethanolamines (NAEs), including *N*-palmitoylethanolamine (PEA), *N*-oleoylethanolamine (OEA) and anandamide, by hydrolysis of the phosphodiester bond between the phosphoglyceride and the *N*-acylethanolamine in *N*-acylphosphatidyl-ethanolamines (NAPEs).[15] Knockout (KO) studies have shown that the conversion of NAPEs to NAEs bearing both saturated and polyunsaturated fatty acyl groups were reduced by 5-fold in brain lysates from mice that genetically lack *Napepld*.[18] In accordance, depleted levels of saturated and mono-unsaturated NAEs were observed in the brain of NAPE-PLD KO mice.[18-20] Surprisingly, anandamide levels were not reduced in all transgenic models, which led to the discovery of alternative biosynthetic pathways for anandamide.[16,18,21-23] However, compensatory pathways render these long-term, constitutive genetic mouse models poorly suited for studying the rapid and dynamic formation of anandamide and its biological role. Thus, a great need exists for pharmacological tools that can help to clarify the function of NAPE-PLD in 'on demand' production of anandamide. Unfortunately, potent CNS-active inhibitors are currently not available. Previously described NAPE-PLD inhibitors lack the potency, selectivity and/or physicochemical properties to function as *in situ* and/or *in vivo* active NAPE-PLD inhibitors.[24-26]

In this chapter, **LEI-401** (Figure 1), which was identified in Chapter 3 as a nanomolar potent NAPE-PLD inhibitor, is profiled in cellular and animal models. **LEI-401** reduced a broad range of NAEs including anandamide in neuronal cells, but not in NAPE-PLD KO cells, thereby confirming 'on-target' activity. Mice administered an intraperitoneal (i.p.) injection of **LEI-401** showed a dose-dependent reduction of anandamide in the brain at 2 hours. Behavioral profiling of **LEI-401**-treated mice showed hypomotility,

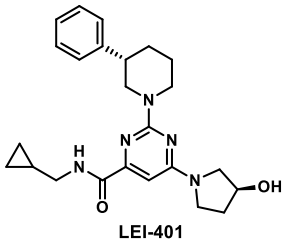

LEI-401

Figure 1. Structure of NAPE-PLD inhibitor **LEI-401.**

hypothermia and antinociception in the hot plate test. Taken together, **LEI-401** demonstrates the crucial role of NAPE-PLD as an anandamide-producing enzyme in the CNS, and points to a role for NAPE-PLD in the acute and dynamic regulation of neurophysiological pain behavior. **LEI-401** opens new opportunities to study anandamide and NAE signaling *in vivo*.

5.2 Results

5.2.1 Profiling the selectivity of LEI-401 for the endocannabinoid system (ECS).

LEI-401 was selected from a NAPE-PLD inhibitor library of pyrimidine-6-carboxamides for further biological profiling due to its optimal potency and physicochemical parameters (described in Chapter 3). First, the activity profile of **LEI-401** for the receptors and metabolic enzymes of the endocannabinoid system was assessed. No inhibitory activities were measured at 10 μM for the cannabinoid receptors type 1 and 2 (CB_1/CB_2) (Table 1) as well as for the enzymes involved in anandamide biosynthesis and degradation, respectively, phospholipase A_2 group IV E (PLA2G4E) and FAAH (Table 2). In addition, **LEI-401** did not inhibit enzymes involved in the biosynthesis and degradation of the other endocannabinoid 2-arachidonoylglycerol (2-AG), including diacylglycerol lipases (DAGLα or DAGLβ), monoacylglycerol lipase (MAGL) and α,β-hydrolase domain 6 (ABHD6) (Table 2).

Table 1. **LEI-401** did not significantly inhibit the CB_1 and CB_2 receptors.

Radioligand displacement at 10 μM **LEI-401** (% ± SD)	
hCB1	hCB2
36 ± 2	47 ± 9
> 50% is considered a target	

Table 2. **LEI-401** showed no inhibitory activity for metabolic enzymes of the ECS. Activities were measured using surrogate or natural substrate assays for DAGLα/β and MAGL, or activity-based protein profiling for PLA2G4E, FAAH and ABHD6.

Remaining enzyme activity at 10 μM **LEI-401** (% ± SD)						
hDAGLα	mDAGLα	mDAGLβ	hMAGL	hPLA2G4E	mFAAH	mABHD6
81 ± 7	76 ± 21	96 ± 23	64 ± 15	89 ± 14	107 ± 14	101 ± 2
< 50% is considered a target						

5.2.2 LEI-401 lowers anandamide levels in WT Neuro-2a, but not in NAPE-PLD KO cells.

Having established that **LEI-401** is a cell-permeable inhibitor that engages with NAPE-PLD (described in Chapter 4), and is selective over the receptors and metabolic enzymes of the ECS, we then investigated whether **LEI-401** inhibited endogenous NAPE-PLD in living cells. To this end, the mouse Neuro-2a neuroblastoma cell line was selected, because it expressed endogenous NAPE-PLD as determined by quantitative PCR (qPCR) (*Napepld*: C_q ± SD = 24.22 ± 0.088, *Hprt* (housekeeping gene): C_q ± SD = 19.48 ± 0.047) and western blot

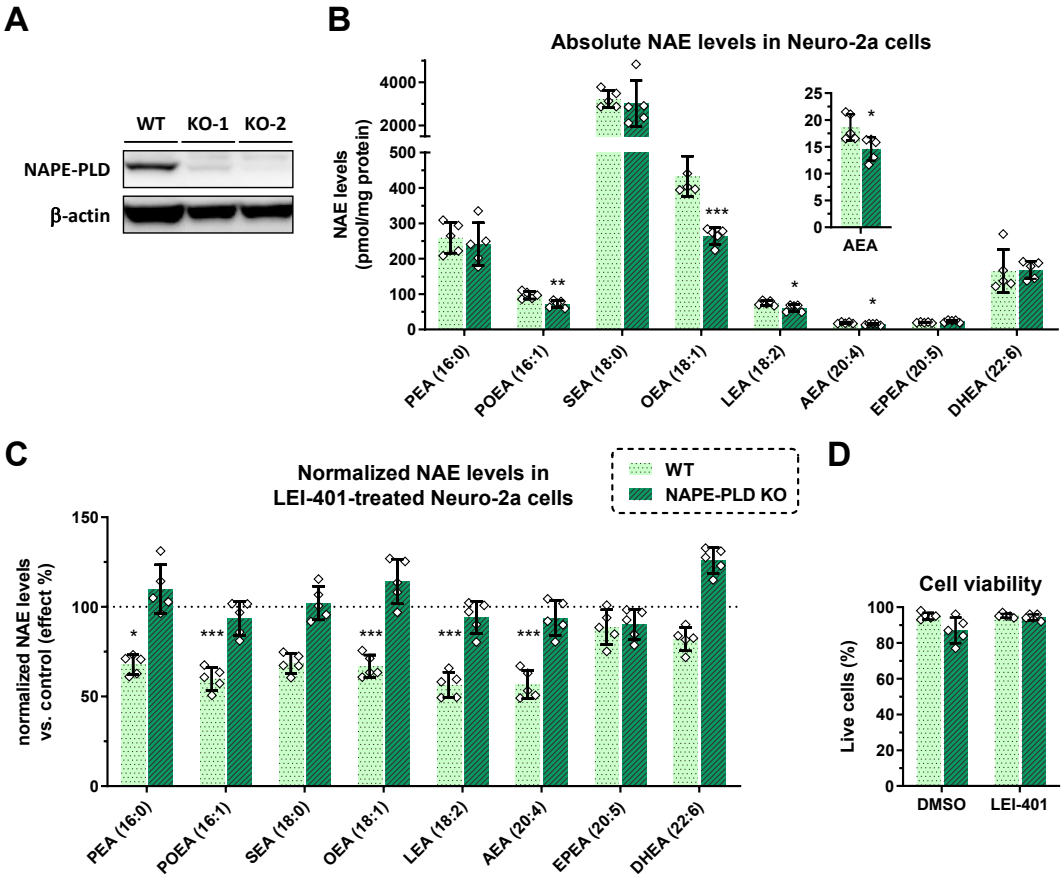

Figure 2. LEI-401 reduces *N*-acylethanolamine (NAE) levels in wild-type (WT) Neuro-2a cells, but not in NAPE-PLD KO cells. **A**) Western blot showing NAPE-PLD protein expression in WT cells, but not in NAPE-PLD knockout cell line KO-2. **B**) Absolute NAE levels of WT and NAPE-PLD KO cells. **C**) Relative NAE levels of WT and NAPE-PLD KO cells treated with **LEI-401** (10 μM, 2 h), represented as effect %. Data were normalized against WT or NAPE-PLD KO cells treated with vehicle (DMSO). Absolute values for all NAEs are depicted in Supplementary Figure 1. **D**) **LEI-401** (10 μM, 2 h) showed no effect on the viability of Neuro-2a WT and NAPE-PLD KO cells. Live cells were identified based on Trypan blue exclusion. Data represent mean values ± SD for 5 biological replicates. *, $P < 0.05$, **, $P < 0.01$, ***, $P < 0.001$ by one-way ANOVA.

using NAPE-PLD antibodies (Figure 2A). Targeted lipidomics on lipid extracts of Neuro-2a cells allowed the quantification of eight different NAEs by liquid chromatography-mass spectrometry (LC-MS) (Figure 2B). As an appropriate negative control, a NAPE-PLD KO cell line was generated using CRISPR-Cas9. Due to single cell heterogeneity of the Neuro-2a cell line, two KO populations were prepared by three sequential rounds of transfections with Cas9 and two different single guide RNAs (sgRNA), which targeted exon 2 (KO-1) or exon 3 (KO-2). The cell line KO-2 showed most efficient ablation of NAPE-PLD protein expression as demonstrated by western blot analysis (Figure 2A). Next, wild-type (WT) and KO cells were incubated with **LEI-401** (10 μM) for 2 h. A significant 2-fold reduction of anandamide was apparent in the WT cells but not in the NAPE-PLD KO cells, indicating that the **LEI-401**-induced reduction in anandamide levels depended on expression of NAPE-PLD in Neuro-2a cells (Figure 2C). **LEI-401**-treated cells did not show any sign of reduced cell viability (Figure 2D). Notably, the smaller but significant decrease of anandamide (~25%) in NAPE-PLD KO cells compared to WT may indicate the occurrence of compensatory mechanisms in the NAPE-PLD KO cells, as also observed by others in *Napepld*-deficient mice (Supplementary Figure 1A).[18] Furthermore, other saturated, mono- and (ω-6)-polyunsaturated NAEs showed a similar 2-fold decrease in WT cells upon **LEI-401** treatment, but not in NAPE-PLD KO cells (Figure 2C, Supplementary Figure 1B-F). (ω-3)-Polyunsaturated EPEA and DHEA did not respond to **LEI-401** treatment (Figure 2C, Supplementary Figure 2G-H). Our data are in line with previously reported biochemical substrate studies using purified recombinant NAPE-PLD and indicate that endogenously expressed NAPE-PLD is responsible for biosynthesis of saturated, mono- and (ω-6)-polyunsaturated NAEs in Neuro-2a cells. The lack of effect on (ω-3)-polyunsaturated NAEs may suggest that these signaling lipids are produced via another pathway. Of note, recently it was found that dietary (ω-3)-polyunsaturated fatty acids augment brain NAE levels in mice via a pathway independent of NAPE-PLD.[27]

LEI-401 also reduced 2-AG and related monoacylglycerols (MAGs) 2-lineoylglycerol (2-LG) and 2-oleoylglycerol (2-OG) in both WT and NAPE-PLD KO cells, indicating a NAPE-PLD-independent mechanism of action (Supplementary Figure 1I-K). Although no evidence was found for direct inhibition of the MAG biosynthetic enzymes DAGLα/β by **LEI-401** (Table 2), possible modulation of the DAGLα/β activity or expression levels via an alternative pathway cannot be ruled out at this point. The elevation of arachidonic acid (AA) in the KO cells compared to WT suggests that NAPE-PLD ablation may have an inflammatory effect (Supplementary Figure 1L), although this AA increase was not observed upon 24 h treatment with or without **LEI-401** (data not shown).

5.2.3 LEI-401 shows high CNS penetration and reduces brain anandamide levels *in vivo*.

Before testing whether **LEI-401** possesses *in vivo* efficacy, its absorption, distribution, metabolism and excretion (ADME) profile was determined. **LEI-401** demonstrated favorable physicochemical properties for oral bioavailability and brain penetration (MW = 422 Da; LogD = 3.3 and topological polar surface area (tPSA) = 80.5 $Å^2$). **LEI-401** had low aqueous solubility (1.7 μg/mL) and permeates well through membranes (PAMPA P_{eff} = 0.37 cm/μs). Clearance in human and mouse microsomes (10 and 42 μL/min/mg protein, respectively) as well as in hepatocytes (6.9 and 28.8 μl/min/10^6 cells, respectively) was moderate, except for the low human microsomal clearance. **LEI-401** exhibited high human and mouse protein binding (> 99.8 %). Of note, it did not interact with either human or mouse PGP-transporter (efflux ratios: 1.7 and 1.8, respectively).

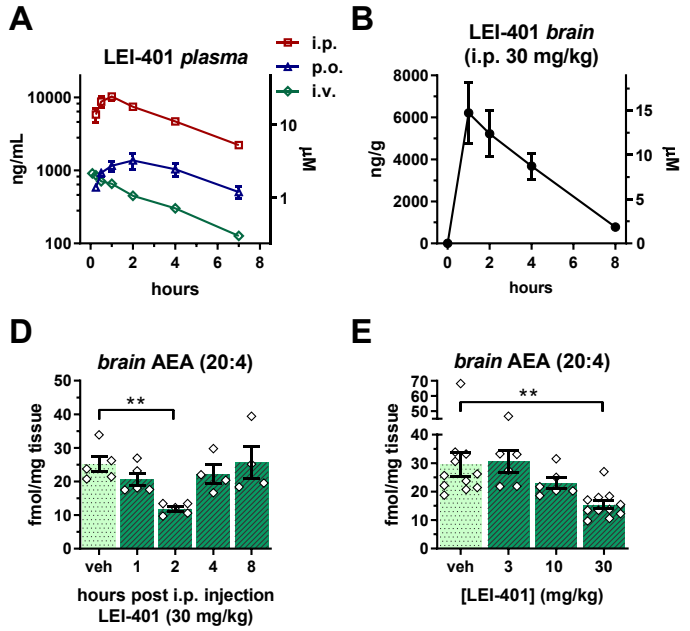

C

	i.v.	p.o.	i.p.
Dose (mg/kg)	**1**	**10**	**30**
CL (mL/min/kg)[a]	5.2	-	-
V_{ss} (L/kg)[b]	1.2	-	-
$t_{1/2}$ (h)[c]	2.7	2.5	ND
C_{max} (ng/mL)[d]	-	1370	10300
t_{max} (h)[e]	-	2	1
AUC_{last} (h*ng/mL)[f]	-	6760	38600
F (%) (AUC_{last})[g]	-	25	48

Figure 3. LEI-401 pharmacokinetic (PK) profile, showing high CNS penetration and dose-dependent reduction of anandamide in mouse brain. **A**) *In vivo* PK of **LEI-401** in plasma of C57BL/6J mice via intraperitoneal (i.p., 30 mg/kg), oral (p.o., 10 mg/kg) or intravenous (i.v., 1 mg/kg) administration. **B**) Brain PK profile of **LEI-401** in C57BL/6J mice after i.p. administration (30 mg/kg). For **A-B**): data represent mean values ± SEM for 3-5 biological replicates per group. **C**) PK parameters of **LEI-401** in C57BL/6J mice after i.p., p.o. or i.v. administration. [a] CL = clearance. [b] V_{ss} = volume of distribution at steady state. [c] $t_{1/2}$ = half-life. [d] C_{max} = maximum plasma drug concentration. [e] t_{max} = time to reach C_{max}. [f] AUC_{last} = area under plasma concentration-time curve from $t_0 \rightarrow t_{last}$. [g] F = bioavailability. **D**) Time-dependent effect of **LEI-401** on brain AEA. C57BL/6J mice i.p. injected with **LEI-401** (30 mg/kg). **E**) Dose-dependent effect of **LEI-401** on brain AEA at 2 h after i.p. administration. For **D-E**): data represent mean values ± SEM for 5-11 biological replicates. **, $P < 0.01$, by one-way ANOVA.

Pharmacokinetic analysis for **LEI-401** in male C57BL/6J mice revealed a low clearance (CL = 5.2 mL/min/kg) and moderate volume of distribution (V_{ss} = 1.2 L/kg), resulting in a half-life of 2.7 h (Figure 3A,C). The low *in vivo* clearance was not expected based on the *in vitro* clearance, but can be explained by the tight protein binding. Bioavailability after oral administration (F_{po}) reached 25% and a more favorable bioavailability was achieved via intraperitoneal (i.p.) injection (F_{ip} = 48%). In both cases good plasma exposures (AUC) were obtained. The brain to plasma ratio was 0.7 at C_{max} (2 h post injection). This led to an excellent brain exposure (> 10 μM) after 30 mg/kg i.p. administration (Figure 3B), which corresponds to approximately 70-fold the mouse NAPE-PLD K_i-value (0.18 μM), and should be sufficient to modulate NAPE-PLD activity in mouse brain.

In view of the encouraging PK properties and brain exposure, **LEI-401** or vehicle was administered to male C57BL/6J mice (30 mg/kg, i.p., single dose) and the mice were sacrificed after 1, 2, 4 or 8 hours to determine whether NAE levels were reduced. To this end, brain NAE levels were analyzed by LC-MS. **LEI-401** induced a significant and time-dependent reduction for anandamide (*P* = 0.0051), which was maximal at 2 h and returned to vehicle level by 4 h (Figure 3D). A similar trend, though not significant, was observed for OEA and DHEA (Supplementary Figure 2A,B). In contrast to long-term ablation of NAPE-PLD as seen in knockout mice[18], these data indicate that acute NAPE-PLD inhibition primarily affects anandamide levels in mouse brain. Next, mice were treated with various doses of **LEI-401** (3, 10 and 30 mg/kg or vehicle, i.p., single dose) and brain lipids were analyzed at 2 h. A dose-dependent reduction of anandamide was observed with a 2-fold decrease apparent at the highest dose (30 mg/kg) (Figure 3E). Other NAE lipid species did not achieve significant reductions at the highest dose (Supplementary Figure 3A-C). Notably, 2-AG was also dose-dependently decreased compared to vehicle-treated animals (Supplementary Figure 3D). Together, these data establish that acute NAPE-PLD inhibition reduces brain anandamide levels and indicate that **LEI-401** can be used to target NAPE-PLD in living animals to investigate the biological role of NAPE-PLD.

5.2.4 LEI-401 produces analgesic effects *in vivo*.

To assess the effect of acute anandamide reduction in the brain, an explorative *in vivo* behavioral profiling study was undertaken in which locomotion, antinociception, body temperature and catalepsy were measured. **LEI-401** treatment (30 mg/kg, i.p., single dose) in male C57BL/6J mice significantly reduced locomotor activity (*P* = 0.039) and decreased body temperature (*P* = 0.0005) at 2 h, while showing no signs of catalepsy in the bar test (Figure 4A-C). An antinociceptive response was observed in the hot plate test of thermal pain sensation, showing elevated latencies (*P* = 0.0087), albeit less pronounced

than a positive control (CP-55,940, a CB_1/CB_2 receptor agonist) (Figure 4D). No antinociception was apparent in the tail-immersion test (Figure 4E). To rule out that **LEI-401** or its metabolites produced these behavioral effects via the CB_1 receptor, the same set of experiments were repeated in CB_1 receptor KO mice. Again, **LEI-401** induced locomotion depression, hypothermia and antinociception in the hot plate assay (Figure 5A-E), indicative of a CB_1 receptor-independent mechanism.

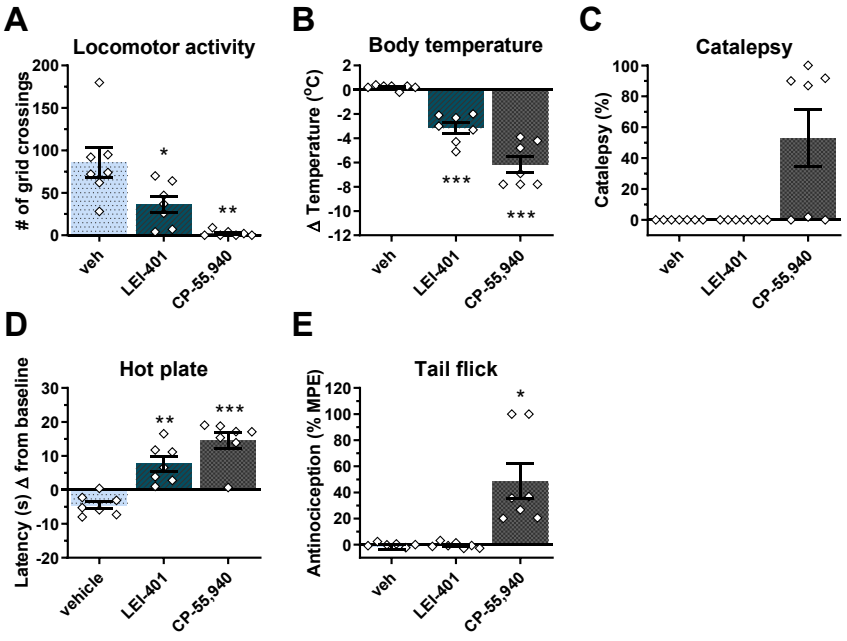

Figure 4. *In vivo* behavioral effects of **LEI-401** in the tetrad test in C57BL/6J mice. **LEI-401** (30 mg/kg, i.p., single dose) produced locomotor depression (**A**) and hypothermia (**B**), but no catalepsy (**C**). Elevated latencies in the hot plate test of thermal pain were observed (**D**), but no antinociception in the tail flick assay (**E**) (% MPE = maximum possible effect %). The CB_1/CB_2 receptor agonist CP-55940 was used as a positive control. Data represent mean values ± SEM for 7-11 biological replicates. *, $P < 0.05$, **, $P < 0.01$, ***, $P < 0.001$ by one-way ANOVA.

5.2.5 LEI-401 reverses LPS-induced allodynia.

The analgesic effect of **LEI-401** observed in the hot plate test, encouraged further investigation into its antinociceptive potential. Therefore, **LEI-401** was tested in a model of inflammatory pain of lipopolysaccharide (LPS)-induced mechanical allodynia in mice. Intraplantar LPS injection (2.5 μg) in the hind paw produced significant allodynic responses compared to vehicle (Figure 6A). **LEI-401** treatment (30 mg/kg, i.p, single dose) 22 h after LPS injection fully reversed LPS-induced allodynia for 2 to 4 h after

administration (P = 0.0027 and 0.0061, respectively), consistent with its PK profile (Figure 3A,B).

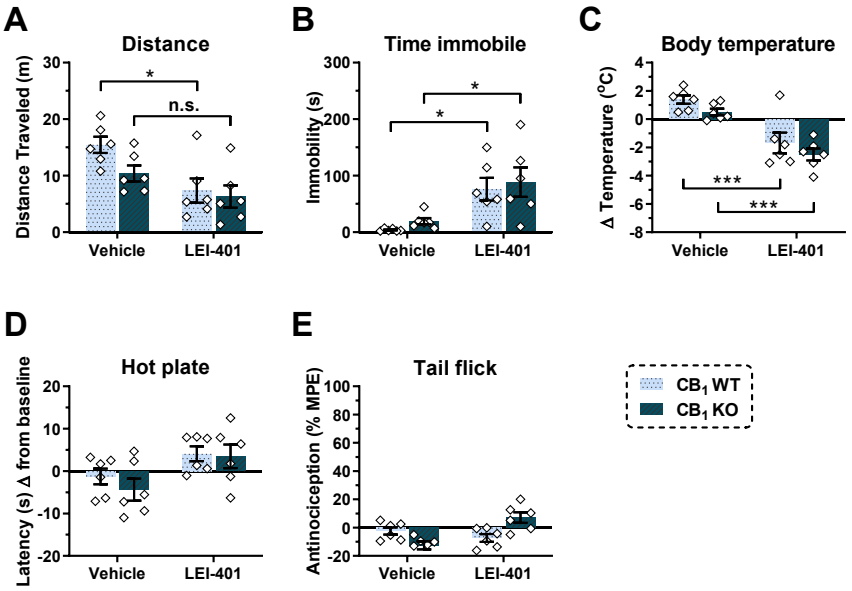

Figure 5. LEI-401-induced behavioral effects were sustained in CB_1 KO mice. **LEI-401** (30 mg/kg, i.p., single dose) induced hypomotility (**A**,**B**), hypothermia (**C**) and antinociception in the hot plate assay (**D**) but not in the tail flick test (**E**). No catalepsy was observed (data not shown). Data represent mean values ± SEM for 6 biological replicates. *, P < 0.05, ***, P < 0.001 by two-way ANOVA.

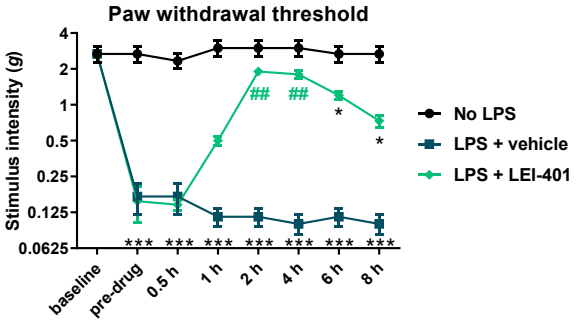

Figure 6. LEI-401 showed antinociception in a mouse model of inflammatory pain. Von Frey nociceptive testing in C57BL/6J mice displayed complete reversal of LPS-induced allodynic pain for 2 to 4 h after **LEI-401** administration (30 mg/kg, i.p., single dose). Data represent mean values ± SEM for 6-8 biological replicates. *, P < 0.05, ***, P < 0.001 compared to 'No LPS' treatment; $^{\#\#}$, P < 0.01 compared to 'LPS + vehicle' by two-way ANOVA.

5.3 Discussion

Anandamide regulates synaptic plasticity in the brain and modulates various physiological and behavioral functions. Inhibitors of its degradation have shed light on its role in pain, energy balance, locomotion and emotional states, such as anxiety. However, assessing the biological consequences of reducing anandamide levels represents an increased challenge because of a lack of selective, CNS-active inhibitors that block *in vivo* anandamide production. In addition, the development of NAPE-PLD KO mice revealed the presence of alternative, compensatory biosynthetic pathways in the brain, which questioned the biological role of NAPE-PLD in anandamide production.[16] Here, we have addressed these important questions by developing the first centrally active NAPE-PLD inhibitor **LEI-401**.

Acute NAPE-PLD inhibition by **LEI-401** in mouse neuronal Neuro-2a cells decreased saturated, mono- and (ω-6)-polyunsaturated NAEs (including anandamide), while leaving (ω-3)-polyunsaturated NAEs unperturbed. This effect was not present in Neuro-2a cells lacking NAPE-PLD, showing the specificity of **LEI-401**. Of note, acute NAPE-PLD inhibition resulted in lower anandamide levels than observed in the NAPE-PLD KO cells, thereby indicating that long-term inactivation of NAPE-PLD in cells also may lead to activation of compensatory pathways (Supplementary Figure 1A). Administration of **LEI-401** to WT mice resulted in a time- and dose-dependent decrease in anandamide content in the brain and influenced nociceptive behavior. These findings provide strong experimental evidence for the biological action of NAPE-PLD in anandamide production in the CNS, support the 'on demand' model of anandamide biosynthesis and reveal a role of NAPE-PLD in complex neurophysiological behavior.

While NAPE-PLD does not show any substrate specificity in biochemical and cellular studies, our findings indicate that primarily anandamide levels are acutely reduced in brains of freely moving mice. The factors that regulate the specific turnover of anandamide over other NAEs remain unknown, but previous studies have shown that anandamide levels are strongly influenced by FAAH activity, the metabolic enzyme of anandamide.[28] The tonic flux of anandamide in the brain undoubtedly depends on the relative contribution of NAPE-PLD and FAAH activity; especially in brain regions were the two enzymes are co-expressed, such as the hippocampus and frontal cortex.[29] In addition, the specific activity and localization of phospholipase and acyltransferases (PLAAT1-5)[30] and the Ca^{2+}-dependent N-acyltransferase (PLA2G4E)[31], enzymes that produce the substrates of NAPE-PLD, represent other determinants in the biosynthesis of NAEs. Lastly, it is possible that the *in vivo* substrate specificity and activity of NAPE-PLD could be controlled by its protein-protein interactions, post-translational modifications (> 10

potential sites for PTMs have been detected (https://www.phosphosite.org) and/or endogenous allosteric modulators. For example, bile acids and polyamines significantly increased NAPE-PLD activity *in vitro*.[17,32,33] Regardless of the precise mechanism that specifically controls anandamide production, our data highlight the importance of NAPE-PLD in the biosynthesis of anandamide in the brain.

LEI-401 elicited hypothermia, hypomotility and antinociception in the hot plate test. This neurophysiological behavior was maintained in CB_1 receptor KO mice, indicating that CB_1 receptor signaling is not involved in the actions of **LEI-401** or its metabolites. This finding contrasts to pharmacological inhibition or deletion of FAAH, in which anandamide elevation produces CB_1 receptor-dependent antinociceptive effects, as evidenced by blockade of the CB_1 receptor with the antagonist rimonabant.[28,34,35] In addition, similar to inhibitors of FAAH[36], **LEI-401** evoked analgesia in a model of inflammatory pain. While the exact molecular mechanism underpinning the neurophysiological behavior of acute NAPE-PLD inhibition is yet unknown, it is interesting to note that anandamide interacts with various other proteins in the CNS, including nuclear receptors (PPAR) and ion channels (e.g. TASK-1, T-type Ca^{2+} channels, NMDA and TRPV1).[9] Furthermore, NAPE-PLD is expressed in nociceptive sensory neurons and thalamus.[37,38] Thus, our data suggest that NAPE-PLD may set an endogenous tone that plays a role in the neural circuitries mediating nociceptive behavior.[38,39] Alternatively, we cannot exclude the possibility that the substrates and other products of NAPE-PLD – NAPEs and phosphatidic acids, respectively – act as signaling molecules in their own right and/or alter (plasma)membrane properties, thereby exerting biological effects.[26,40] It will be critical to evaluate the **LEI-401**-induced effects in NAPE-PLD KO mice, to confirm an on-target mechanism of action. Nevertheless, our data indicate that **LEI-401** produces useful analgesic effects *in vivo* that will be the focus of future research.

Finally, our studies suggest that **LEI-401** and the developed NAPE-PLD photoaffinity probes (Chapter 4) constitute a valuable toolbox to study various aspects of NAPE-PLD and anandamide biology both in animal and cellular models. Although **LEI-401** was shown to be selective in a chemical proteomics setting (Chapter 4) and did not inhibit DAGLα and DAGLβ, the enzymes responsible for the production of the other endocannabinoid 2-AG, it depleted 2-AG, 2-LG and 2-OG content in Neuro-2a cells in a NAPE-PLD-independent manner. Furthermore, **LEI-401** dose-dependently reduced brain 2-AG levels in mice. These observations indicate that **LEI-401** or its metabolites may have off-target activities and highlight the need of combining chemical probes with genetic models to study on-target and off-target interactions of pharmacological agents. Second generation NAPE-PLD inhibitors will benefit from the identification of the off-targets. From a translational

perspective, it will be interesting to study NAPE-PLD inhibitors in various animal models of human disease, such as metabolic syndrome[41], type II diabetes[42], neurodegeneration[43,44], anxiety[45], inflammatory and neuropathic pain[38], stress-related disorders[46], chronic liver disease[47] and cancer[48]. The NAPE-PLD inhibitor reported in this study provides the first opportunity to study the central role of NAPE-PLD in anandamide biosynthesis in the brain of living animals in an acute and dynamic manner, thereby revealing the function of this enzyme in acute nociceptive behavior. It is envisioned that **LEI-401** may help to validate NAPE-PLD as a therapeutic target and serve as a starting point for the discovery of future drug candidates.

Acknowledgements

Annelot van Esbroeck is kindly acknowledged for generating the NAPE-PLD KO cell lines. Andrea Martella, Marjolein Soethoudt, Ming Jiang, Tom van der Wel, Timo Wendel and Anthe Janssen are acknowlegded for performing biochemical assays. Vasudev Kantae, Xinyu Di and Thomas Hankemeier are kindly thanked for determining cellular lipid levels. The ADME profile and *in vivo* PK of **LEI-401** was measured at Hoffman-La Roche under supervision of Matthias Wittwer and Uwe Grether, for which they are kindly acknowledged. Resat Cinar, Zoltan Varga, Janos Paloczi, Joshua Park, Pal Pacher, Mohammed Mustafa, Giulia Donvito and Aron Lichtman are kindly thanked for profiling **LEI-401** *in vivo* and performing lipidomics and behavioral experiments.

5.4 Experimental section

A. Biological procedures

Cell culture

Neuro-2a cells (ATCC) were cultured at 37 ^{o}C and 7% CO_2 in DMEM (Sigma Aldrich, D6546) with GlutaMax (2 mM), penicillin (100 μg/ml), streptomycin (100 μg/ml) and 10% New Born Calf serum. Cells were passaged twice a week to appropriate confluence by thorough pipetting.

Cell lysate preparation

Neuro-2a cells were harvested by removal of culture medium and addition of cold PBS. Cells were pipetted loose, transferred to 50 mL tubes, centrifuged (10 min, 200 g, 4 ^{o}C) and the supernatant was removed. The cell pellets were flash frozen in liquid N_2 and stored at -80 ^{o}C. Whole cell lysates were prepared by addition of lysis buffer: 20 mM HEPES, 2 mM DTT, 0.25 M sucrose, 1 mM $MgCl_2$, 2.5 U/mL benzonase. Cells were homogenized by thorough pipetting and incubated for 30 minutes on ice. Protein concentrations were determined using a Bradford assay (Bio-Rad) and samples were stored at -80 ^{o}C.

qPCR

RNA isolation and cDNA synthesis: Total RNA from Neuro-2a cells was extracted using Trizol reagent (ThermoFisher Scientific). Once isolated, RNA concentration and purity was determined by Nanodrop (Denovix Inc.). Subsequently cDNA synthesis was carried out with Maxima H minus first strand cDNA synthesis kit (ThermoFisher Scientific) according to the manufacturer's instructions.

qPCR analysis: 10 ng of input cDNA was analyzed using SybrGreen qPCR master mix (Biotool) in combination with CFX96 optical thermal cycler (Bio-Rad). Data analysis was performed using CFX Manager software (Bio-Rad). The housekeeping gene hypoxanthine guanine phosphoribosyl transferase (*Hprt*) was used as a control. Data are expressed in quantitation cycles (C_q) and standard deviation of three technical replicates.

Table S1. Primer sequences of *Napepld* and *Hprt* used for qPCR.

Gene	Forward (5'-3')	Reverse (5'-3')	Accession number
Napepld	AGCGCCAAGCTATCAGTATCC	ACGTCCTCCTCTAGTCTGTAATC	NM_178728
Hprt	TTGACACTGGTAAAACAATGC	GCCTGTATCCAACACTTCG	NM_013556

Western blot

Cell lysates were denatured with 4x Laemmli buffer (stock concentrations: 240 mM Tris-HCl pH 6.8, 8% w/v SDS, 40% v/v glycerol, 5% v/v β-mercaptoethanol, 0.04% v/v bromophenol blue, 30 min, rt) and 10-20 μg per sample was resolved on a 10% acrylamide SDS-PAGE gel (180 V, 75 min). Proteins were transferred from the gel to a 0.2 μm PVDF membrane using a Trans-Blot® Turbo (Bio-Rad). The membranes were washed with TBS (50 mM Tris-HCl pH 7.5, 150 mM NaCl) and blocked with 5% milk in TBST (50 mM Tris-HCl pH 7.5, 150 mM NaCl, 0.05% Tween 20) 1 h at rt or overnight at 4 °C. Primary antibodies against NAPE-PLD (Abcam, ab95397, 1:200, in TBST) and β-actin (Abcam, ab8226, 1:5000 in 5% milk in TBST) were incubated 1 h at rt or overnight at 4 °C. Membranes were washed with TBST and incubated with secondary antibodies: for NAPE-PLD, goat-anti-rabbit-HRP (Santa Cruz, sc-2030, 1:2000 in 5% milk in TBST); for β-actin, goat-anti-mouse-HRP (Santa Cruz, sc-2005, 1:5000 in 5% milk in TBST). All secondary antibodies were incubated 1 h at rt or overnight at 4 °C. Membranes were washed with TBST and TBS. The blot was developed in the dark using a luminol solution (10 mL, 1.4 mM luminol in Tris-HCl pH 8.8), ECL enhancer (100 μL, 6.7 mM *para*-hydroxycoumaric acid in DMSO) and H_2O_2 (3 μL, 30% w/w in H_2O). Chemiluminescence was visualized using a ChemiDoc™ Imaging System (Bio-Rad). Band intensity was normalized to β-actin using ImageLab software (Bio-Rad).

CB_1 and CB_2 receptor radioligand displacement assay

The hCB_1 and hCB_2 receptor radioligand displacement assays were performed as described in Chapter 2.

Natural substrate-based fluorescence assay DAGLα

The human or mouse DAGLα activity assay was performed as described in Chapter 2.

Surrogate substrate-based fluorescence assay DAGLβ

The hDAGLβ activity assay was performed as described in Chapter 2.

Natural substrate-based fluorescence assay MAGL

The hMAGL activity assay was performed as described in Chapter 2.

Activity-based protein profiling for FAAH, ABHD6, ABHD12 and PLA2G4E activity

Gel-based activity-based protein profiling (ABPP) was performed as described in Chapter 2.

Generation of Neuro-2a NAPE-PLD KO populations

sgRNA selection: two sgRNA's, located in exon 2 and 3 with high efficiency and specificity as predicted by CHOPCHOP v2 online web tool (http://chopchop.cbu.uib.no)[49] were selected. Guides were cloned into the BbsI restriction site of plasmid px330-U6-Chimeric_BB-CBh-hSpCas9 (gift from Feng Zhang, Addgene plasmid #42230) as previously described.[50,51] The sgRNA targeting exon 3 yielded higher knockout efficiency as determined by western blot and in the T7E1-assays. This population was used for further experiments.

Sequential transfection: Neuro-2a cells were transfected sequentially (3 times within the course of 10 days) to yield populations with a high knockout efficiency. Cells were seeded at day 0, day 3 and day 6 and transfected at day 1, day 4, and day 7. Samples for T7E1 assays were harvested at day 2, day 5, day 11 and after several weeks of culturing the cells. One day prior to the first transfection, Neuro-2a cells were seeded to a 6 wells plate to reach 80-90% confluence at the time of transfection. Prior to transfection, culture medium was aspirated and 2 mL of fresh medium was added. A 5:1 (m/m) mixture of polyethyleneimine (PEI) (17.5 μg/well) and plasmid DNA (3.5 μg/well) was prepared in serum free culture medium (250 μL each) and incubated (15 min, rt). Transfection was performed by dropwise addition of the PEI/DNA mixture to the cells. 24 h post-transfection the culture medium was refreshed, a small amount of cells was harvested for analysis by T7E1 assay and ABPP while the remainder was kept in culture under standard conditions for following transfections. After three transfection rounds, the cells were cultured according to standard protocol.

T7E1 assay: genomic DNA was obtained by mixing 50 μL QuickExtract™ (Epicentre) with cell pellet (~10% of a well, from a 6 well plate). The samples were incubated at 65 °C for 6 min, mixed by vortexing and then incubated at 98 °C for 2 min. Genomic DNA extracts were diluted in sterile water and directly used in PCR reactions. Genomic PCR reactions were performed on 2.5-5 μL isolated genomic DNA extract using Phusion High-Fidelity DNA Polymerase (Thermo Fisher) in Phusion HF buffer in a final volume of 20 μL, for primers see Table S2.

For the T7E1 assay, genomic PCR products were denatured and reannealed in a thermocycler using the following program: 5 min at 95 °C, 95 to 85 °C using a ramp rate of -2 °C/s, 85 to 25 °C using a ramp rate of -0.2 °C/s. To annealed PCR product (8.5 μL) was added NEB2 buffer (1 μL) and T7 endonuclease I (5 U, 0.5 μL; New England Biolabs), followed by incubation at 37 °C for 30 min. Digested PCR products were analyzed using agarose gel electrophoresis with ethidium bromide staining. Agarose gels were analyzed using ImageLab Software (Bio-Rad) and CRISPR gene editing efficiency was expressed as percentage T7E cleavage (volume integral of digested bands / volume integral all bands * 100 %).

Table S2. Primer sequences for sgRNA and T7E1 assay.

sgRNA Target	Primer sequence*	
***Napepld* – Exon 2 (KO-1)**	Top:	CACCGATAGCTTGGCGCTGGAGAC
	Bottom:	AAACGTCTCCAGCGCCAAGCTATC
	Forward:	ccgaggtaccataCTTAAAATCCTGTTTTGCAGCC
	Reverse:	caacaccggtatcGTGGTCATAGGACCCATTTGTT
***Napepld* – Exon 3 (KO-2)**	Top:	CACCAGTTCGCTTATTGTACACGG
	Bottom:	AAACCCGTGTACAATAAGCGAACT
	Forward:	ccgaggtaccataAGGTACACGCTGTGTAAGAGCA
	Reverse:	caacaccggtatcAAGGACCAAACCTTTTTCCAAT

* The *Napepld*-specific sequence is underlined.

B. Targeted lipidomics in Neuro-2a cells

The targeted lipidomics experiments are based on previously reported methods with small alterations.[52]

Sample preparation

$2 \cdot 10^6$ Neuro-2a cells (grown at 37 °C, 7% CO_2) were seeded 1 day before treatment in 6 cm dishes. Before treatment, cells were washed twice with warm PBS and then treated with vehicle or compound (10 μM, 0.1% DMSO) in 3 mL medium without serum (2 h at 37 °C, n = 5 per condition). Washing with cold PBS (1x) followed by harvesting in 1.5 mL Eppendorf tubes and centrifugation (10 min, 1500 rpm). PBS was removed and the cell pellets were flash frozen with liquid nitrogen and stored at -80 °C. Live cell count with trypan blue was performed after compound treatment to test for cell viability. 10% of each cell sample (collected during harvesting) was used to determine the protein concentration using a Bradford assay (Bio-Rad) for normalization after lipid measurements.

Lipid extraction

Lipids extraction was performed on ice. In brief, cell pellets with $2 \cdot 10^6$ cells were transferred to 1.5 mL Eppendorf tubes, spiked with 10 μL each of deuterium labeled internal standard mix for endocannabinoids (*N*-arachidonoylethanolamine (AEA)-d8, *N*-docosahexaenoylethanolamine (DHEA)-d4, 2-arachidonoylglycerol (2-AG)-d8, *N*-stearoylethanolamine (SEA)-d3, *N*-palmitoylethanolamine (PEA)-d4, *N*-linoleoylethanolamine (LEA)-d3 and *N*-oleoylethanolamine (OEA)-d4), and negative polar lipids (fatty acid (FA)17:0-d33), followed by the addition of ammonium acetate buffer (100 μL, 0.1 M, pH 4). After extraction with methyl *tert*-butyl ether (MTBE, 1 mL), the tubes were thoroughly mixed for 4 min using a bullet blender at medium speed (Next Advance Inc., Averill park, NY, USA), followed by a centrifugation step (5,000 *g*, 12 min, 4 °C). Then 925 μL of the upper MTBE layer was transferred into clean 1.5 mL Eppendorf tubes. Samples were dried in a speed-vac followed by reconstitution in acetonitrile/water (50 μL, 90 : 10, v/v). The samples were centrifuged (14,000 *g*, 3 min, 4 °C) and transferred into LC-MS vials. Each sample was injected on two different lipidomics platforms: endocannabinoids (5 μL) and negative polar lipids (8 μL).

LC-MS/MS analysis for endocannabinoids

A targeted analysis of endocannabinoids and related NAEs (*N*-acylethanolamines) was measured using an Acquity UPLC I class binary solvent manager pump (Waters, Milford, USA) in conjugation with AB SCIEX 6500 quadrupole ion trap (QTRAP) (AB Sciex, Massachusetts, USA). Separation was performed with an Acquity HSS T3 column (1.2 x 100 mm, 1.8 μm) maintained at 40 °C. The aqueous mobile phase A consisted of 2 mM ammonium formate and 10 mM formic acid, and the organic mobile phase B was acetonitrile. The flow rate was set to 0.4 ml/min; initial gradient conditions were 55% B held for 2 min and linearly ramped to 100% B over 6 minutes and held for 2 min; after 10 s the system returned to initial conditions and held 2 min before next injection. Electrospray ionization-MS was operated in positive mode for measurement of endocannabinoids and NAEs, and a selective Multiple Reaction Mode (sMRM) was used for quantification.

LC-MS/MS analysis for negative polar lipids

This method is measured on an Acquity UPLC binary solvent manager 8 pump (Waters) coupled to an Agilent 6530 electrospray ionization quadrupole time-of-flight (ESI-Q-TOF, Agilent, Jose, CA, USA) high resolution mass spectrometer using reference mass correction. The chromatographic separation was achieved on an Acquity HSS T3 column (1.2 x 100 mm, 1.8 μm) maintained at 40 °C for both methods. The negative apolar lipids that constitute free fatty acids were separated with a flow of 0.4 mL/min over 15 min gradient. In negative mode, the aqueous mobile phase A consisted of 5:95 (v/v) acetonitrile:H_2O with 10 mM ammonium formate, and the organic mobile phase B consisted of 99% (v/v) methanol with 10 mM ammonium formate.

Statistical analysis

Absolute values of lipid levels were corrected using the measured protein concentrations. Data were tested for significance with GraphPad v6 using one-way ANOVA with Tukey correction for multiple comparisons. *P*-values < 0.05 were considered significant.

C. *In vitro* absorption, distribution, metabolism and excretion (ADME) profile of **LEI-401**.

Kinetic aqueous solubility (LYSA = LYophilization Solubility Assay)

The solubility of **LEI-401** in phosphate buffer at pH 6.5 from an evaporated 10 mM DMSO compound stock solution was measured. Two aliquots of the test compound were dried and dissolved in phosphate buffer at pH 6.5. The solutions were then filtered and diluted (3 different dilution levels for each compound) before RapidFire MS analysis was performed. Each test compound was quantified using a 6-point calibration curve prepared with the same DMSO starting solution.

Passive membrane permeability (PAMPA)

PAMPA (Parallel Artificial Membrane Permeability Assay) is a method which determines the permeability of substances from a donor compartment, through a lipid-infused artificial membrane into an acceptor compartment. Read-out is a permeation coefficient P_{eff} drug as well as test compound concentrations in donor, membrane and acceptor compartments. The assay was performed as described elsewhere.[53]

Microsomal clearance

The microsomal clearance assay was performed as previously described.[54] Pooled commercially available microsome preparations from male mouse microsomes (C57BL/6J, Lot 4339006) were purchased from Corning Incorporated (Woburn, USA)). For human, ultra-pooled liver microsomes (150 mixed gender donors, BD UltraPool HLM 150, Lot 38289) were purchased to account for the biological variance *in vivo* from human liver tissues. For the microsome incubations (incubation buffer 0.1 M phosphate buffer pH 7.4), 96-deep well plates were applied, which were incubated at 37 ^{o}C on a TECAN (Tecan Group Ltd, Switzerland) equipped with Te-Shake shakers and a warming device (Tecan Group Ltd, Switzerland). The NADPH regenerating system consisted of 30 mM glucose-6-phosphate disodium salt hydrate; 10 mM NADP; 30 mM $MgCl_2$ x 6 H_2O and 5 μg/μL glucose-6-phosphate dehydrogenase (Roche Diagnostics) in 0.1 M potassium phosphate buffer pH 7.4. Incubations of **LEI-401** at 1 μM in microsome incubations of 0.5 μg/μL plus cofactor NADPH were performed in 96-well plates at 37 ^{o}C. After 1, 3, 6, 9, 15, 25, 35 and 45 minutes 40 μL incubation solutions were transferred and quenched with 3:1 (v/v) acetonitrile containing internal standards. Samples were then cooled and centrifuged before analysis by LC-MS/MS. Log peak area ratios (test compound peak area / internal standard peak area) were plotted against incubation time using a linear fit. The calculated slope was used to determine the intrinsic clearance: CL_{int} (μL/min/mg protein) = -slope (min^{-1}) * 1000 / [protein concentration (μg/μL)].

Hepatocyte clearance

The hepatocyte clearance assay was performed as previously described.[55] For animals, hepatocyte suspension cultures were either freshly prepared by liver perfusion studies or prepared from cryopreserved hepatocyte batches (pooled C57BL6 mouse hepatocytes were purchased from BioreclamationIVT (NY, USA)). For human, commercially available, pooled (5-20 donors), cryopreserved human hepatocytes from non-transplantable liver tissues were used. For the suspension cultures, Nunc U96 PP-0.5 mL (Nunc Natural, 267245) plates were used, which were incubated in a Thermo Forma incubator from Fischer Scientific (Wohlen, Switzerland) equipped with shakers from Variomag® Teleshake shakers (Sterico, Wangen, Switzerland) for maintaining cell dispersion. The cell culture medium was William's media supplemented with Glutamine, antibiotics, insulin, dexamethasone and 10% FCS. Incubations of a test compound at 1 μM

test concentration in suspension cultures of $1{\cdot}10^6$ cells/mL (~1 μg/μL protein concentration) were performed in 96-well plates and shaken at 900 rpm for up to 2 hours in a 5% CO_2 atmosphere at 37 °C. After 3, 6, 10, 20, 40, 60 and 120 minutes 100 μL cell suspension in each well is quenched with 200 μL methanol containing an internal standard. Samples are then cooled and centrifuged before analysis by LC-MS/MS. Log peak area ratios (test compound peak area / internal standard peak area) or concentrations were plotted against incubation time with a linear fit. The slope of the fit was used to calculate the intrinsic clearance: CL_{int} (μL/min/$1{\cdot}10^6$ cells) = -slope (min-1) * 1000 / [$1{\cdot}10^6$ cells].

Plasma protein binding

The plasma protein binding assay was performed as previously described.[56,57] Pooled and frozen plasma from human (HMPLEDTA, Lot BRH1060627) and mouse (MSEPLEDTA3-C57, Lot MSE196204) were obtained from BioreclamationIVT (NY, USA). The Teflon equilibrium dialysis plate (96-well, 150 μL, half-cell capacity) and cellulose membranes (12–14 kDa molecular weight cut-off) were purchased from HT-Dialysis (Gales Ferry, Connecticut). Both biological matrix and phosphate buffer pH were adjusted to 7.4 on the day of the experiment. The determination of unbound compound was performed using a 96-well format equilibrium dialysis device with a molecular weight cut-off membrane of 12 to 14 kDa. The equilibrium dialysis device itself was made of Teflon to minimize non-specific binding of the test substance. Compounds were tested in cassettes of 2-5 with an initial total concentration of 1000 nM, one of the cassette compounds being the positive control diazepam. Equal volumes of matrix samples containing substances and blank dialysis buffer (Soerensen buffer at pH 7.4) were loaded into the opposite compartments of each well. The dialysis block was sealed and kept for 5 hours at a temperature of 37 °C and 5% CO_2 environment in an incubator. After this time, equilibrium has been reached for the majority of small molecule compounds with a molecular weight of <600. The seal was then removed and matrix and buffer from each dialysis was prepared for analysis by LC-MS/MS. All protein binding determinations were performed in triplicates. The integrity of membranes was tested in the HTDialysis device by determining the unbound fraction values for the positive control diazepam in each well. At equilibrium, the unbound drug concentration in the biological matrix compartment of the equilibrium dialysis apparatus was the same as the concentration of the compound in the buffer compartment. Thus, the percent unbound fraction (f_u) was calculated by determining the compound concentrations in the buffer and matrix compartments after dialysis as follows: $\%f_u$ = 100 * buffer concentration after dialysis / matrix concentration after dialysis. The device recovery was checked by measuring the compound concentrations in the matrix before dialysis and calculating the percent recovery (mass balance). The recovery must be within 80% to 120% for data acceptance.

LogD-assay

For the determination of the octanol/water distribution coefficient (logD), the Carrier-Mediated Distribution System (CAMDIS)-assay was used as described elsewhere.[58]

P-glycoprotein active efflux assay

P-glycoprotein (permeability-glycoprotein, abbreviated as 'P-gp' also known as multidrug resistance protein 1 (MDR1)) is the most studied and best characterized drug transporter. The P-gp assay evaluates the ability of test compounds to serve as a P-gp substrate. The assay was performed as described elsewhere.[59]

D. *In vivo* pharmacokinetics of **LEI-401**.

Subjects

Male C57BL/6J mice (Jackson Laboratory, Bar Harbor, Maine, USA) served as subjects for the *in vivo* pharmacokinetic and brain lipid analysis of **LEI-401**. Animal protocols were approved by the Institutional Animal Care and Use Committee at National Institute on Alcohol Abuse and Alcoholism, National Institute of

Health and Bundesamt für Lebensmittelsicherheit und Veterinärwesen (BLV) der Schweizerischen Eidgenossenschaft.

Pharmacokinetic analysis of LEI-401 (mouse plasma)

Test compounds were formulated according to respective protocols either by dissolution (i.v.) or in a glass potter until homogeneity was achieved (p.o. and i.p.). Formulations were injected i.v. using a 30G needle in the lateral tail vein mice yielding a 1 mg/kg-dose. For p.o. applications, animals were gavaged (yielding a 10 mg/kg dose) and for i.p. applications the compounds were injected into the abdomen (yielding a 30 mg/kg dose). At the following time points blood was drawn into EDTA: 0.083, 0.25, 0.5, 1, 2, 4, 7, 24 h (for p.o. and i.p. the first time point was omitted). Three animals each were used for the i.v. and p.o. arm and 6 animals were used in the i.p. arm. Animals were distributed randomly over the time course and at each time point, a volume of 100 μL of blood was taken. Quantitative plasma measurement of the compound was performed by LC-MS/MS analysis. Pharmacokinetic analysis was performed using Phoenix WinNonlin 6.4 software using a non-compartmental approach consistent with the route of administration. For assessment of the exposure C_{max}, T_{max}, AUC and bioavailability were determined from the plasma concentration profiles. Parameters (CL, V_{ss}, $t_{1/2}$) were estimated using nominal sampling times relative to the start of each administration.

Pharmacokinetic analysis of LEI-401 (mouse brain)

Mice were injected with **LEI-401** (30 mg/kg, i.p., single dose) dissolved in sterile DMSO (D2650 Sigma, MO, USA) and mixed with Tween-80 and distilled H_2O at a ratio of 1:1:8. Mice were sacrificed after 1, 2, 4 and 8 h. Brain samples were rapidly collected, washed in ice cold saline, blotted dry, frozen in liquid N_2 and stored at -80 ^{o}C until further analysis. Brain levels of **LEI-401** were quantified by LC-MS/MS using an Agilent 6410 triple quadrupole mass spectrometer (Agilent Technologies, USA) coupled with an Agilent 1200 LC system (Agilent Technologies, Germany). Chromatographic and mass spectrometer conditions were set as described previously.[60] Chromatographic separation was obtained using 2.5 μl samples injected onto a Zorbax SB-C18 rapid resolution HT column (2.1 mm × 50 mm, 1.8 Micron, Agilent). The mass spectrometer was set for electrospray ionization in positive ion mode. The source parameters were as follows: capillary voltage, 4000 V; gas temperature, 350 ^{o}C; drying gas, 10 liters/min; nitrogen was used as the nebulizing gas with a pressure of 40 psig. Collision-induced dissociation (CID) energy was performed by using nitrogen. Levels of **LEI-401** were analyzed by multiple reactions monitoring (MRM). Mass spectrometric conditions were optimized for **LEI-401** with injection of synthetic standard by using MassHunter Workstation Optimizer software (Agilent Technologies, USA). The molecular ion and fragments for **LEI-401** measured were as follows: m/z 422.26→70.1 and 422.26→137 (CID-energy: 56 V and 40 V, respectively). The amounts of **LEI-401** in the samples were determined against standard curves. Values are expressed as ng/g in wet brain tissue weight.

Lipid measurements in mouse brain

Levels of NAEs, 2-AG and arachidonic acid were measured by stable isotope dilution liquid chromatography/tandem mass spectrometry (LC-MS/MS) as described previously.[61]

Statistical analysis

Data were tested for significance with GraphPad v6 using one-way ANOVA with Dunnett's correction for multiple comparisons. *P*-values < 0.05 were considered significant.

E. *In vivo* behavioral assays.

Subjects

Male C57BL/6J mice (Jackson Laboratory, Bar Harbor, Maine, USA) and male and female CB_1 KO and WT mice (VCU transgenic core, Richmond, Virginia, USA) served as subjects for *in vivo* nociceptive testing. The animal protocols were approved by the Institutional Animal Care and Use Committee at Virginia Commonwealth University in accordance with the National Institutes of Health Guide for the Care and Use of Laboratory Animals.[62] All studies involving animals are reported in accordance with the ARRIVE guidelines for reporting experiments involving animals.[63]

Drugs

LEI-401 was synthesized as described in Chapter 3 and the Drug Supply Program at the National Institute on Drug Abuse (Bethesda, MD) provided CP-55,940. **LEI-401** and CP-55,940 were dissolved in respective vehicles consisting of a ratio 1:1:8 ratio of DMSO, Tween 80 and distilled H_2O, and a 1:1:18 ratio of ethanol, emulphor-620 (Rhodia, Cranbury, NJ) and saline (0.9% NaCl). All injections were administered via the i.p. route of administration in a volume of 0.01 ml/g of body mass.

Hot plate nociceptive testing

Mice were placed on a 52 ^{o}C surface of the hot plate (IITC Life Science Inc., Woodland Hills, CA) and the latency to display jumping behavior or licking or shaking of a hind paw was scored during a 30 s observation period. The experimenter used a stopwatch to score latencies to the nearest 0.01 s and was blinded to injection condition. Each mouse was given a pre-injection hot plate test and a second hot plate test 120 min after **LEI-401** (30 mg/kg) administration or 30 min after CP-55,940 (10 mg/kg) administration.

Statistical analysis: nociceptive behavior was expressed as post-injection hot plate latency minus pre-injection latency and are reported as the mean ± SEM difference scores in seconds. ANOVA was used to test **LEI-401** and CP-55,940 vs. vehicle in C57BL/6J mice and Dunnett's test was used for post hoc analysis. Two-way ANOVA was used to evaluate **LEI-401** vs. vehicle in CB_1 KO vs. WT mice. Differences were considered significant at $P < 0.05$.

Evaluation of LEI-401 in body temperature, locomotor behavior, catalepsy and tail immersion assays.

LEI-401 was tested for hypothermia, locomotor depression, catalepsy and antinociception in the tail flick assay as described elsewhere.[64]

Evaluation of LEI-401 in LPS mouse model of inflammatory pain

The LPS-induced allodynia assay was performed as previously described.[64] Mice were given an injection of 2.5 μg of LPS from *Escherichia coli* (026:B6, Sigma), in 20 μL of physiological sterile saline (Hospira Inc., Lake Forest, IL, USA) into the plantar surface of the right hind paw. As previously reported, this dose of LPS elicits mechanical allodynia without producing measurable increases in paw thickness.[65] Mice were returned to their home cages after the LPS injection. 22 hours following LPS administration, each mouse was given an intraperitoneal (i.p.) injection of **LEI-401** (30 mg/kg) or vehicle and tested for mechanical allodynia at 0.5, 1, 2, 4, 6 and 8 h post injection.

Behavioral assessment of mechanical allodynia

Baseline responses to light mechanical touch were assessed using von Frey filaments following habituation to the testing environment. In brief, mice were acclimated to the testing conditions in which they were given a daily 15 min habituation session for 2 days. They were placed under an inverted wire mesh basket, which allowed unrestricted air flow, that was on top of a wire mesh screen, with spaces 0.5 mm apart. During acclimation and testing, each mouse was unrestrained and singly housed. The von Frey test utilizes a series of calibrated monofilaments, (2.83–4.31 log stimulus intensity; North Coast Medical, Morgan Hills, CA,

USA) applied randomly to the left and right plantar surfaces of the hind paw for 3 touches, 1/2 seconds apart. Lifting, licking, or shaking the paw was considered a response.

References

1. Piomelli, D. The molecular logic of endocannabinoid signalling. *Nature Reviews Neuroscience* **4**, 873 (2003).
2. Hannun, Y.A. & Obeid, L.M. Principles of bioactive lipid signalling: lessons from sphingolipids. *Nature Reviews Molecular Cell Biology* **9**, 139 (2008).
3. Kano, M., Ohno-Shosaku, T., Hashimotodani, Y., Uchigashima, M. & Watanabe, M. Endocannabinoid-mediated control of synaptic transmission. *Physiological Reviews* **89**, 309-380 (2009).
4. Rouzer, C.A. & Marnett, L.J. Endocannabinoid oxygenation by cyclooxygenases, lipoxygenases, and cytochromes P450: cross-talk between the eicosanoid and endocannabinoid signaling pathways. *Chemical Reviews* **111**, 5899-5921 (2011).
5. Alger, B.E. & Kim, J. Supply and demand for endocannabinoids. *Trends in Neurosciences* **34**, 304-315 (2011).
6. Hampson, A.J., Bornheim, L.M., Scanziani, M., Yost, C.S., Gray, A.T., Hansen, B.M., Leonoudakis, D.J. & Bickler, P.E. Dual effects of anandamide on NMDA receptor-mediated responses and neurotransmission. *Journal of Neurochemistry* **70**, 671-676 (1998).
7. Chemin, J., Monteil, A., Perez-Reyes, E., Nargeot, J. & Lory, P. Direct inhibition of T-type calcium channels by the endogenous cannabinoid anandamide. *The EMBO Journal* **20**, 7033-7040 (2001).
8. Maingret, F., Patel, A.J., Lazdunski, M. & Honoré, E. The endocannabinoid anandamide is a direct and selective blocker of the background K^+ channel TASK-1. *The EMBO Journal* **20**, 47-54 (2001).
9. van der Stelt, M., Trevisani, M., Vellani, V., De Petrocellis, L., Schiano Moriello, A., Campi, B., McNaughton, P., Geppetti, P. & Di Marzo, V. Anandamide acts as an intracellular messenger amplifying Ca^{2+} influx via TRPV1 channels. *The EMBO Journal* **24**, 3026-3037 (2005).
10. Piomelli, D. & Sasso, O. Peripheral gating of pain signals by endogenous lipid mediators. *Nature Neuroscience* **17**, 164 (2014).
11. Lutz, B., Marsicano, G., Maldonado, R. & Hillard, C.J. The endocannabinoid system in guarding against fear, anxiety and stress. *Nature Reviews Neuroscience* **16**, 705 (2015).
12. Witkamp, R.F. The role of fatty acids and their endocannabinoid-like derivatives in the molecular regulation of appetite. *Molecular Aspects of Medicine* (2018).
13. Turcotte, C., Chouinard, F., Lefebvre Julie, S. & Flamand, N. Regulation of inflammation by cannabinoids, the endocannabinoids 2-arachidonoyl-glycerol and arachidonoyl-ethanolamide, and their metabolites. *Journal of Leukocyte Biology* **97**, 1049-1070 (2015).
14. Maccarrone, M. Metabolism of the endocannabinoid anandamide: open questions after 25 years. *Frontiers in Molecular Neuroscience* **10** (2017).
15. Okamoto, Y., Morishita, J., Tsuboi, K., Tonai, T. & Ueda, N. Molecular characterization of a phospholipase D generating anandamide and its congeners. *Journal of Biological Chemistry* **279**, 5298-5305 (2004).
16. Hussain, Z., Uyama, T., Tsuboi, K. & Ueda, N. Mammalian enzymes responsible for the biosynthesis of *N*-acylethanolamines. *Biochimica et Biophysica Acta (BBA) - Molecular and Cell Biology of Lipids* **1862**, 1546-1561 (2017).
17. Magotti, P., Bauer, I., Igarashi, M., Babagoli, M., Marotta, R., Piomelli, D. & Garau, G. Structure of human *N*-acylphosphatidylethanolamine-hydrolyzing phospholipase D: regulation of fatty acid ethanolamide biosynthesis by bile acids. *Structure* **23**, 598-604 (2015).

18. Leung, D., Saghatelian, A., Simon, G.M. & Cravatt, B.F. Inactivation of *N*-acyl phosphatidylethanolamine phospholipase D reveals multiple mechanisms for the biosynthesis of endocannabinoids. *Biochemistry* **45**, 4720-4726 (2006).
19. Tsuboi, K., Okamoto, Y., Ikematsu, N., Inoue, M., Shimizu, Y., Uyama, T., Wang, J., Deutsch, D.G., Burns, M.P., Ulloa, N.M., Tokumura, A. & Ueda, N. Enzymatic formation of *N*-acylethanolamines from *N*-acylethanolamine plasmalogen through *N*-acylphosphatidylethanolamine-hydrolyzing phospholipase D-dependent and -independent pathways. *Biochimica et Biophysica Acta (BBA) - Molecular and Cell Biology of Lipids* **1811**, 565-577 (2011).
20. Leishman, E., Mackie, K., Luquet, S. & Bradshaw, H.B. Lipidomics profile of a NAPE-PLD KO mouse provides evidence of a broader role of this enzyme in lipid metabolism in the brain. *Biochimica et Biophysica Acta (BBA) - Molecular and Cell Biology of Lipids* **1861**, 491-500 (2016).
21. Blankman, J.L. & Cravatt, B.F. Chemical probes of endocannabinoid metabolism. *Pharmacological Reviews* **65**, 849-871 (2013).
22. Simon, G.M. & Cravatt, B.F. Characterization of mice lacking candidate *N*-acyl ethanolamine biosynthetic enzymes provides evidence for multiple pathways that contribute to endocannabinoid production in vivo. *Molecular BioSystems* **6**, 1411-1418 (2010).
23. Simon, G.M. & Cravatt, B.F. Endocannabinoid biosynthesis proceeding through glycerophospho-*N*-acyl ethanolamine and a role for α/β-hydrolase 4 in this pathway. *Journal of Biological Chemistry* **281**, 26465-26472 (2006).
24. Petersen, G., Pedersen, A.H., Pickering, D.S., Begtrup, M. & Hansen, H.S. Effect of synthetic and natural phospholipids on *N*-acylphosphatidylethanolamine-hydrolyzing phospholipase D activity. *Chemistry and Physics of Lipids* **162**, 53-61 (2009).
25. Scott, S.A., Spencer, C.T., O'Reilly, M.C., Brown, K.A., Lavieri, R.R., Cho, C.-H., Jung, D.-I., Larock, R.C., Brown, H.A. & Lindsley, C.W. Discovery of desketoraloxifene analogues as inhibitors of mammalian, Pseudomonas aeruginosa, and NAPE phospholipase D enzymes. *ACS Chemical Biology* **10**, 421-432 (2015).
26. Castellani, B., Diamanti, E., Pizzirani, D., Tardia, P., Maccesi, M., Realini, N., Magotti, P., Garau, G., Bakkum, T., Rivara, S., Mor, M. & Piomelli, D. Synthesis and characterization of the first inhibitor of *N*-acylphosphatidylethanolamine phospholipase D (NAPE-PLD). *Chemical Communications* **53**, 12814-12817 (2017).
27. Lin, L., Metherel, A.H., Kitson, A.P., Alashmali, S.M., Hopperton, K.E., Trépanier, M.-O., Jones, P.J. & Bazinet, R.P. Dietary fatty acids augment tissue levels of n-acylethanolamines in *N*-acylphosphatidylethanolamine phospholipase D (NAPE-PLD) knockout mice. *The Journal of Nutritional Biochemistry* **62**, 134-142 (2018).
28. Cravatt, B.F., Demarest, K., Patricelli, M.P., Bracey, M.H., Giang, D.K., Martin, B.R. & Lichtman, A.H. Supersensitivity to anandamide and enhanced endogenous cannabinoid signaling in mice lacking fatty acid amide hydrolase. *Proceedings of the National Academy of Sciences* **98**, 9371-9376 (2001).
29. Egertová, M., Simon, G.M., Cravatt, B.F. & Elphick, M.R. Localization of *N*-acyl phosphatidylethanolamine phospholipase D (NAPE-PLD) expression in mouse brain: a new perspective on *N*-acylethanolamines as neural signaling molecules. *Journal of Comparative Neurology* **506**, 604-615 (2008).
30. Uyama, T., Tsuboi, K. & Ueda, N. An involvement of phospholipase A/acyltransferase family proteins in peroxisome regulation and plasmalogen metabolism. *FEBS Letters* **591**, 2745-2760 (2017).
31. Ogura, Y., Parsons, W.H., Kamat, S.S. & Cravatt, B.F. A calcium-dependent acyltransferase that produces N-acyl phosphatidylethanolamines. *Nature Chemical Biology* **12**, 669 (2016).
32. Margheritis, E., Castellani, B., Magotti, P., Peruzzi, S., Romeo, E., Natali, F., Mostarda, S., Gioiello, A., Piomelli, D. & Garau, G. Bile acid recognition by NAPE-PLD. *ACS Chemical Biology* **11**, 2908-2914 (2016).
33. Liu, Q., Tonai, T. & Ueda, N. Activation of *N*-acylethanolamine-releasing phospholipase D by polyamines. *Chemistry and Physics of Lipids* **115**, 77-84 (2002).

34. Kathuria, S., Gaetani, S., Fegley, D., Valiño, F., Duranti, A., Tontini, A., Mor, M., Tarzia, G., Rana, G.L., Calignano, A., Giustino, A., Tattoli, M., Palmery, M., Cuomo, V. & Piomelli, D. Modulation of anxiety through blockade of anandamide hydrolysis. *Nature Medicine* **9**, 76 (2002).
35. Long, J.Z., Nomura, D.K., Vann, R.E., Walentiny, D.M., Booker, L., Jin, X., Burston, J.J., Sim-Selley, L.J., Lichtman, A.H., Wiley, J.L. & Cravatt, B.F. Dual blockade of FAAH and MAGL identifies behavioral processes regulated by endocannabinoid crosstalk in vivo. *Proceedings of the National Academy of Sciences* **106**, 20270 (2009).
36. Lamont, B., G, K.S., A, A.R., L, B.J., Z, L.J., Cyrine, E., L, B.D., F, C.B. & H, L.A. The fatty acid amide hydrolase (FAAH) inhibitor PF-3845 acts in the nervous system to reverse LPS-induced tactile allodynia in mice. *British Journal of Pharmacology* **165**, 2485-2496 (2012).
37. Morishita, J., Okamoto, Y., Tsuboi, K., Ueno, M., Sakamoto, H., Maekawa, N. & Ueda, N. Regional distribution and age-dependent expression of *N*-acylphosphatidylethanolamine-hydrolyzing phospholipase D in rat brain. *Journal of Neurochemistry* **94**, 753-762 (2005).
38. Sousa-Valente, J., Varga, A., Torres-Perez, J.V., Jenes, A., Wahba, J., Mackie, K., Cravatt, B., Ueda, N., Tsuboi, K., Santha, P., Jancso, G., Tailor, H., Avelino, A. & Nagy, I. Inflammation of peripheral tissues and injury to peripheral nerves induce differing effects in the expression of the calcium-sensitive *N*-arachydonoylethanolamine-synthesizing enzyme and related molecules in rat primary sensory neurons. *Journal of Comparative Neurology* **525**, 1778-1796 (2017).
39. Gauldie, S.D., McQueen, D.S., Pertwee, R. & Chessell, I.P. Anandamide activates peripheral nociceptors in normal and arthritic rat knee joints. *British Journal of Pharmacology* **132**, 617-621 (2001).
40. Wellner, N., Diep, T.A., Janfelt, C. & Hansen, H.S. *N*-Acylation of phosphatidylethanolamine and its biological functions in mammals. *Biochimica et Biophysica Acta (BBA) - Molecular and Cell Biology of Lipids* **1831**, 652-662 (2013).
41. Geurts, L., Everard, A., Van Hul, M., Essaghir, A., Duparc, T., Matamoros, S., Plovier, H., Castel, J., Denis, R.G.P., Bergiers, M., Druart, C., Alhouayek, M., Delzenne, N.M., Muccioli, G.G., Demoulin, J.-B., Luquet, S. & Cani, P.D. Adipose tissue NAPE-PLD controls fat mass development by altering the browning process and gut microbiota. *Nature Communications* **6**, 6495 (2015).
42. Jourdan, T., Godlewski, G., Cinar, R., Bertola, A., Szanda, G., Liu, J., Tam, J., Han, T., Mukhopadhyay, B., Skarulis, M.C., Ju, C., Aouadi, M., Czech, M.P. & Kunos, G. Activation of the Nlrp3 inflammasome in infiltrating macrophages by endocannabinoids mediates beta cell loss in type 2 diabetes. *Nature Medicine* **19**, 1132 (2013).
43. Hansen, H.H., Ikonomidou, C., Bittigau, P., Hansen, S.H. & Hansen, H.S. Accumulation of the anandamide precursor and other *N*-acylethanolamine phospholipids in infant rat models of in vivo necrotic and apoptotic neuronal death. *Journal of Neurochemistry* **76**, 39-46 (2001).
44. Janfelt, C., Wellner, N., Leger, P.-L., Kokesch-Himmelreich, J., Hansen, S.H., Charriaut-Marlangue, C. & Hansen, H.S. Visualization by mass spectrometry of 2-dimensional changes in rat brain lipids, including *N*-acylphosphatidylethanolamines, during neonatal brain ischemia. *The FASEB Journal* **26**, 2667-2673 (2012).
45. Dincheva, I., Drysdale, A.T., Hartley, C.A., Johnson, D.C., Jing, D., King, E.C., Ra, S., Gray, J.M., Yang, R., DeGruccio, A.M., Huang, C., Cravatt, B.F., Glatt, C.E., Hill, M.N., Casey, B.J. & Lee, F.S. FAAH genetic variation enhances fronto-amygdala function in mouse and human. *Nature Communications* **6**, 6395 (2015).
46. Bowles, N.P., Karatsoreos, I.N., Li, X., Vemuri, V.K., Wood, J.-A., Li, Z., Tamashiro, K.L.K., Schwartz, G.J., Makriyannis, A.M., Kunos, G., Hillard, C.J., McEwen, B.S. & Hill, M.N. A peripheral endocannabinoid mechanism contributes to glucocorticoid-mediated metabolic syndrome. *Proceedings of the National Academy of Sciences* **112**, 285-290 (2015).
47. Caraceni, P., Viola, A., Piscitelli, F., Giannone, F., Berzigotti, A., Cescon, M., Domenicali, M., Petrosino, S., Giampalma, E., Riili, A., Grazi, G., Golfieri, R., Zoli, M., Bernardi, M. & Di Marzo, V. Circulating and

hepatic endocannabinoids and endocannabinoid-related molecules in patients with cirrhosis. *Liver International* **30**, 816-825 (2010).

48. Mukhopadhyay, B., Schuebel, K., Mukhopadhyay, P., Cinar, R., Godlewski, G., Xiong, K., Mackie, K., Lizak, M., Yuan, Q., Goldman, D. & Kunos, G. Cannabinoid receptor 1 promotes hepatocellular carcinoma initiation and progression through multiple mechanisms. *Hepatology* **61**, 1615-1626 (2015).
49. Labun, K., Montague, T.G., Gagnon, J.A., Thyme, S.B. & Valen, E. CHOPCHOP v2: a web tool for the next generation of CRISPR genome engineering. *Nucleic Acids Research* **44**, W272-W276 (2016).
50. Cong, L., Ran, F.A., Cox, D., Lin, S., Barretto, R., Habib, N., Hsu, P.D., Wu, X., Jiang, W., Marraffini, L.A. & Zhang, F. Multiplex genome engineering using CRISPR/Cas systems. *Science* **339**, 819-823 (2013).
51. Ran, F.A., Hsu, P.D., Wright, J., Agarwala, V., Scott, D.A. & Zhang, F. Genome engineering using the CRISPR-Cas9 system. *Nature Protocols* **8**, 2281 (2013).
52. van Esbroeck, A.C.M., Janssen, A.P.A., Cognetta, A.B., Ogasawara, D., Shpak, G., van der Kroeg, M., Kantae, V., Baggelaar, M.P., de Vrij, F.M.S., Deng, H., Allarà, M., Fezza, F., Lin, Z., van der Wel, T., Soethoudt, M., Mock, E.D., den Dulk, H., Baak, I.L., Florea, B.I., Hendriks, G., De Petrocellis, L., Overkleeft, H.S., Hankemeier, T., De Zeeuw, C.I., Di Marzo, V., Maccarrone, M., Cravatt, B.F., Kushner, S.A. & van der Stelt, M. Activity-based protein profiling reveals off-target proteins of the FAAH inhibitor BIA 10-2474. *Science* **356**, 1084-1087 (2017).
53. Kansy, M., Senner, F. & Gubernator, K. Physicochemical high throughput screening: parallel artificial membrane permeation assay in the description of passive absorption processes. *Journal of Medicinal Chemistry* **41**, 1007-1010 (1998).
54. Di, L., Keefer, C., Scott, D.O., Strelevitz, T.J., Chang, G., Bi, Y.-A., Lai, Y., Duckworth, J., Fenner, K., Troutman, M.D. & Obach, R.S. Mechanistic insights from comparing intrinsic clearance values between human liver microsomes and hepatocytes to guide drug design. *European Journal of Medicinal Chemistry* **57**, 441-448 (2012).
55. LeCluyse, E.L., Witek, R.P., Andersen, M.E. & Powers, M.J. Organotypic liver culture models: meeting current challenges in toxicity testing. *Critical Reviews in Toxicology* **42**, 501-548 (2012).
56. Banker, M.J., Clark, T.H. & Williams, J.A. Development and validation of a 96-well equilibrium dialysis apparatus for measuring plasma protein binding. *Journal of Pharmaceutical Sciences* **92**, 967-974 (2003).
57. Zamek-Gliszczynski, M.J., Ruterbories, K.J., Ajamie, R.T., Wickremsinhe, E.R., Pothuri, L., Rao, M.V.S., Basavanakatti, V.N., Pinjari, J., Ramanathan, V.K. & Chaudhary, A.K. Validation of 96-well equilibrium dialysis with non-radiolabeled drug for definitive measurement of protein binding and application to clinical development of highly-bound drugs. *Journal of Pharmaceutical Sciences* **100**, 2498-2507 (2011).
58. Wagner, B., Fischer, H., Kansy, M., Seelig, A. & Assmus, F. Carrier Mediated Distribution System (CAMDIS): A new approach for the measurement of octanol/water distribution coefficients. *European Journal of Pharmaceutical Sciences* **68**, 68-77 (2015).
59. Poirier, A., Cascais, A.-C., Bader, U., Portmann, R., Brun, M.-E., Walter, I., Hillebrecht, A., Ullah, M. & Funk, C. Calibration of in vitro multidrug resistance protein 1 substrate and inhibition assays as a basis to support the prediction of clinically relevant interactions in vivo. *Drug Metabolism and Disposition* **42**, 1411-1422 (2014).
60. Cinar, R., Iyer, M.R., Liu, Z., Cao, Z., Jourdan, T., Erdelyi, K., Godlewski, G., Szanda, G., Liu, J., Park, J.K., Mukhopadhyay, B., Rosenberg, A.Z., Liow, J.-S., Lorenz, R.G., Pacher, P., Innis, R.B. & Kunos, G. Hybrid inhibitor of peripheral cannabinoid-1 receptors and inducible nitric oxide synthase mitigates liver fibrosis. *JCI Insight* **1** (2016).
61. Mukhopadhyay, B., Cinar, R., Yin, S., Liu, J., Tam, J., Godlewski, G., Harvey-White, J., Mordi, I., Cravatt, B.F., Lotersztajn, S., Gao, B., Yuan, Q., Schuebel, K., Goldman, D. & Kunos, G. Hyperactivation of anandamide synthesis and regulation of cell-cycle progression via cannabinoid type 1 (CB_1) receptors in the regenerating liver. *Proceedings of the National Academy of Sciences* **108**, 6323-6328 (2011).

62. Council, N.R. *Guide for the care and use of laboratory animals: eighth edition*. (The National Academies Press, Washington, DC; 2011).
63. Kilkenny, C., Browne, W., Cuthill, I.C., Emerson, M. & Altman, D.G. Animal research: Reporting in vivo experiments: The ARRIVE guidelines. *British Journal of Pharmacology* **160**, 1577-1579 (2010).
64. Wilkerson, J.L., Donvito, G., Grim, T.W., Abdullah, R.A., Ogasawara, D., Cravatt, B.F. & Lichtman, A.H. Investigation of diacylglycerol lipase alpha inhibition in the mouse lipopolysaccharide inflammatory pain model. *Journal of Pharmacology and Experimental Therapeutics* **363**, 394-401 (2017).
65. Booker, L., Kinsey, S.G., Abdullah, R.A., Blankman, J.L., Long, J.Z., Ezzili, C., Boger, D.L., Cravatt, B.F. & Lichtman, A.H. The fatty acid amide hydrolase (FAAH) inhibitor PF-3845 acts in the nervous system to reverse LPS-induced tactile allodynia in mice. *British Journal of Pharmacology* **165**, 2485-2496 (2012).

Supplementary Information

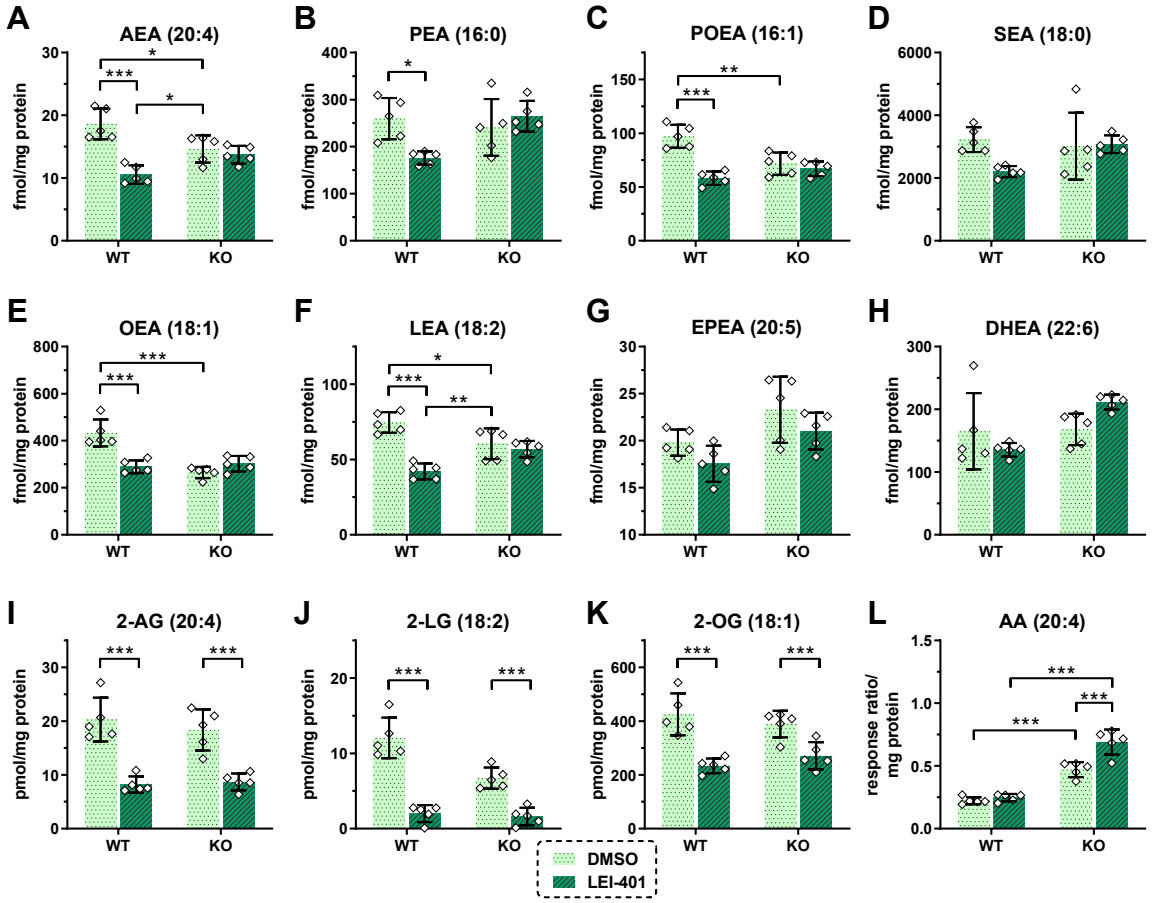

Supplementary Figure 1. Absolute lipid levels of NAEs, monoacylglycerols (MAGs) and arachidonic acid (AA) in Neuro-2a wild-type (WT) and NAPE-PLD knockout (KO) cells treated with **LEI-401** (10 μM) for 2 h. **A**) Anandamide (AEA, 20:4-ω-6), **B**) *N*-palmitoylethanolamine (PEA, 16:0), **C**) *N*-palmitoleoylethanolamine (POEA, 16:1-ω-9), **D**) *N*-stearoylethanolamine (SEA, 18:0), **E**) *N*-oleoylethanolamine (OEA, 18:1-ω-9), **F**) *N*-linoleoylethanolamine (LEA, 18:2-ω-6), **G**) *N*-eicosapentaenoylethanolamine (EPEA, 20:5-ω-3), **H**) *N*-docosahexaenoylethanolamine (DHEA, 22:6-ω-3), **I**) 2-arachidonoylglycerol (2-AG, 20:4-ω-6), **J**) 2-linoleoylglycerol (2-LG, 18:2-ω-6), **K**) 2-oleoylglycerol (2-OG, 18:1-ω-9) and **L**) arachidonic acid (AA, 20:4-ω-6). Data represent mean values ± SD for 5 biological replicates. *, $P < 0.05$, **, $P < 0.01$, ***, $P < 0.001$ by one-way ANOVA.

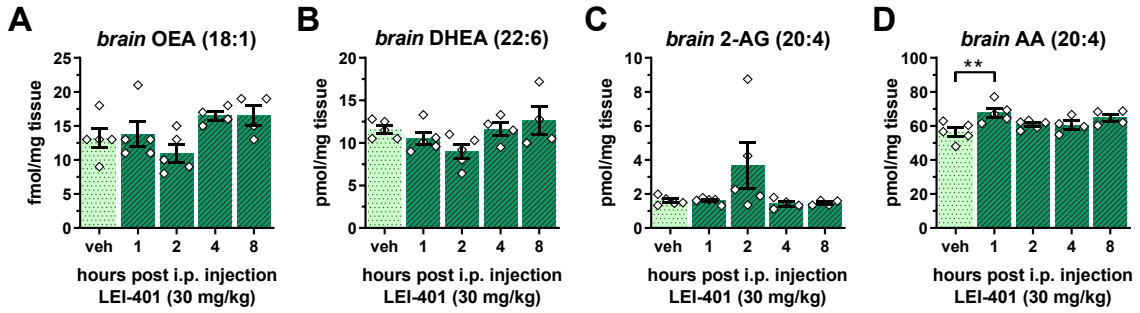

Supplementary Figure 2. *In vivo* treatment of **LEI-401** (30 mg/kg, i.p., single dose) showed time-dependent effects on brain NAEs and other bioactive lipids in C57BL/6J mice. **A**) OEA, **B**) DHEA, **C**) 2-AG, **D**) AA. Data represent mean values ± SEM for 5-6 biological replicates. **, $P < 0.01$ by one-way ANOVA.

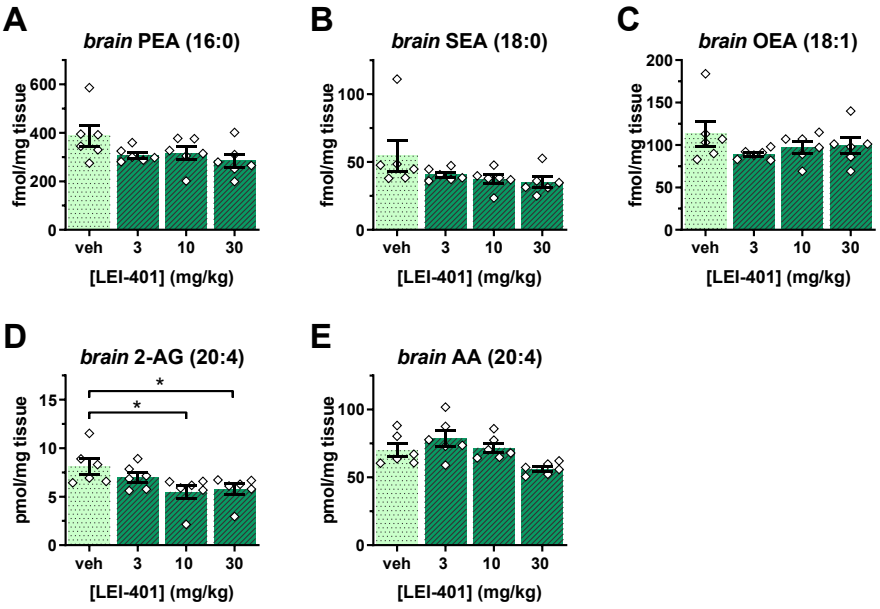

Supplementary Figure 3. *In vivo* treatment of **LEI-401** revealed dose-dependent effects on brain NAEs and other bioactive lipids in C57BL/6J mice 2 h after i.p. administration. **A**) PEA, **B**) SEA, **C**) OEA, **D**) 2-AG and **E**) AA. Data represent mean values ± SEM for 5-6 biological replicates. *, $P < 0.05$, **, $P < 0.01$ by one-way ANOVA.